NANO LETTERS

pubs.acs.org/NanoLett

Hierarchical TiO_2 Photoanode for Dye-Sensitized Solar Cells

F. Sauvage,[†] F. Di Fonzo,[*,‡,§] A. Li Bassi,[‡,§] C. S. Casari,[‡,§] V. Russo,[§] G. Divitini,[||] C. Ducati,[||] C. E. Bottani,[‡,§] P. Comte,[†] and M. Graetzel[*,†]

[†]Laboratoire de Photonique et Interfaces, Institut des Sciences et Ingénieurie Chimiques, Ecole Polytechnique Fédérale de Lausanne (EPFL), Station 6, CH-1015, Lausanne, Switzerland, [‡]Center for Nano Science and Technology of IIT@PoliMI, Via Pascoli 70/3 20133 Milano, Italy, [§]Dipartimento di Energia and NEMAS - Center for NanoEngineered Materials and Surfaces, Politecnico di Milano; via Ponzio 34/3, 20133 Milano, Italy, and [||]Department of Materials Science and Metallurgy, University of Cambridge, Pembroke Street, CB3 3QZ Cambridge, United Kingdom

ABSTRACT Hierarchical or one-dimensional architectures are among the most exciting developments in material science these recent years. We present a nanostructured TiO_2 assembly combining these two concepts and resembling a forest composed of individual, high aspect-ratio, treelike nanostructures. We propose to use these structures for the photoanode in dye-sensitized solar cells, and we achieved 4.9% conversion efficiency in combination with C101 dye. We demonstrate this morphology beneficial to hamper the electron recombination and also mass transport control in the mesopores when solvent-free ionic liquid electrolyte is used.

KEYWORDS Dye-sensitized solar cell, pulsed laser deposition, TiO_2, C101 dye, photoanode

Research aimed at tailoring materials at the nanoscale has paved the way toward new challenges, in particular in the domain of photoelectrochemistry with the development of water photoelectrolysis for hydrogen production[1] or dye-sensitized solar cells (DSSC) which, in principle, mimic the natural photosynthesis in the leaf.[2] After twenty years of research, DSSC technology shows enough maturity for viable outdoor application as witnessed by the recent achievements on single-junction lab cells exceeding 11% power conversion efficiency (PCE),[3−5] 9% stable[6] or on the production of W-contact submodules showing more than 8%.[7] The low environmental impact, low cost, short energy pay-back time (<1 year), low sensitivity to temperature changes or to light angle of incidence, performance maintained at low irradiance and easy elaboration upon flexible substrates are some promising features guaranteed by DSSC over the other alternatives. Nevertheless, a substantial amount of research work is still needed to fill the gap between today's benchmark conversion efficiency and the Shockley-Queiser limit of $\eta = 32\%$ predicted for a single junction cell.[8] The TiO_2 electrode sensitized by a chromophore based on organic donor−acceptor units, or polypyridil Ru^{+II}-containing complex, represents the heart of the device, where exciton generation and carrier transport constitute separate processes. High-conversion performance is achieved when the electron diffusion length is much greater than the TiO_2 film thickness. This is the case when charge transport is promoted against carrier recombination either via the oxidized dye (S^+) or via the reduced electrolyte I_3^-, competitive processes that arise in the ms time domain.[9] The enhancement of the electron diffusion length by reducing the dimensionality of the TiO_2 photoanode has been successfully demonstrated by means of vertically aligned TiO_2 nanotubes or nanowires produced by electrochemical anodization from Ti metal,[10−14] using softer methods like hydrothermal growth[15] or, more recently, DC sputtering upon TCO.[16] Another explored route is the synthesis of hierarchical meso-architectures combining efficient light trapping and high surface area for dye absorption.[17,18] In this work, we present a novel photoanode architecture combining these two approaches synthesized by pulsed laser deposition (PLD). This established technique is well-known for its versatility to grow a wide variety of materials.[19] Recently, it has been demonstrated that it is possible to grow complex, high surface area films of different oxides via a fine control of the growth parameters (e.g., background gas pressure, laser fluence, deposition temperature, or time).[20−24] In particular, some of us have shown that the variation of the plasma expansion dynamics by means of a reactive atmosphere during the ablation process allows a fine-tuning of morphology and crystalline structure of titanium oxide films at the nano- and mesoscale.[25] Herein, we introduce a novel architecture for the DSSC photoanode which consists of hierarchical assemblies of nanocrystalline particles of anatase TiO_2, morphologically resembling a tree, giving rise in fine to a forestlike architecture. The trees are directly grown on TiO_2-coated fluorine-doped tin oxide (FTO) at room temperature by ablation of a Ti target in a background O_2 atmosphere (details about material synthesis can be found in ref 25). The height of the trees and hence film

* To whom correspondence should be addressed. E-mail: (M.G.) michael.graetzel@epfl.ch; (F.D.F.) fabio.difonzo@iit.it.

Received for review: 04/6/2010
Published on Web: 06/21/2010

DOI: 10.1021/nl101198b | *Nano Lett.* **2010,** *10,* 2562–2567

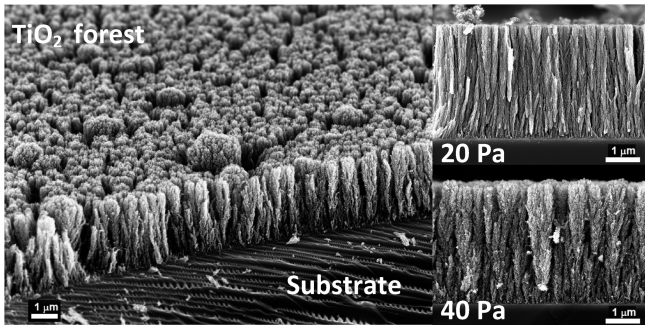

FIGURE 1. Scanning electron micrographs of PLD TiO_2 films: (left) overview of a film deposited at 40 Pa; (right) cross sections of films deposited at 20 and 40 Pa.

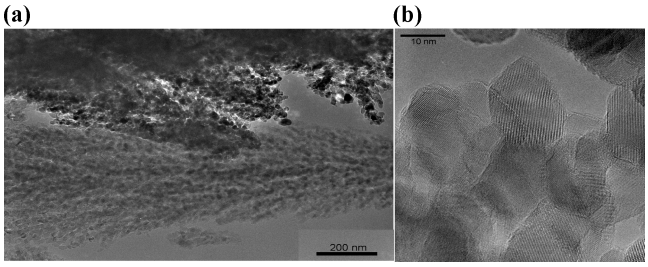

FIGURE 2. (a) Bright-field TEM image of a single tree (section, horizontal) and (b) high-resolution TEM image of a cluster of anatase TiO_2 nanoparticles.

thickness increases linearly with deposition time. Depending on experimental conditions, a deposition rate up to 1 μm/min can be achieved over a 10×5 cm^2. As-deposited films are amorphous and annealing in air at 500 °C is usually performed to obtain the desired anatase crystalline phase. Figure 1 shows field-emission scanning electron microscopy (FESEM) micrographs of films deposited at different oxygen pressures, namely 20 and 40 Pa. From the cross sections presented in Figure 1b,c, the forestlike morphology of the film is evident for both oxygen pressures. The hierarchical, treelike morphology of the primary aggregates can be observed in the transmission electron microscopy (TEM) micrograph in Figure 2a for the film grown at 20 Pa. Here the growth axis of the tree is horizontal, from right to left. TiO_2 nanocrystal arrays 10−40 nm in diameter represent the branches, which reach 500 nm in length and form an angle of 15−20 degrees with the tree's growth axis. These images show the anisotropic growth and multiscale structuring of the trees with a length in the micrometer scale and made up of branches in the 100 nm scale, constituted by an assembly of nanoparticles in the 10 nm scale. SEM images also suggest that as the film grows thicker the tree structures become more open, which is typical of low-energy deposition processes from the gas phase, and that surface area increases more than linearly with thickness. High-resolution imaging (Figure 2b) shows highly crystalline, faceted particles in the anatase phase in agreement to the recorded X-ray diffraction pattern.[23] The size distribution of the individual nanocrystals is centered at about 25 nm, ranging from 10 to 40 nm. Similar considerations apply to the film grown at the higher pressure, except that the branches and trees packing density are both lower thus decreasing the average film density. The effect of oxygen pressure on nucleation and growth processes of TiO_2 films is thoroughly detailed in ref 23. In brief, pulsed laser deposition at low pressures (<10 Pa) yields dense films, while at high pressures (>100 Pa) free nanoparticles are formed in the gas phase that can assemble in an aerogel-like morphology, attaining a porosity of 94%. In between these two asymptotic regimes, well documented in the literature, a narrow window of operating conditions[19] allows the growth of high aspect ratio, hierarchical microstructures via self-assembly from the gas phase. The two types of film shown (grown at 20 and 40 Pa) are a typical example of this fascinating hierarchical tree microstructure. Brunauer−Emmett−Teller (BET) analysis based on N_2 adsorption has been used to determine surface area and the pore size distribution using the Barrett−Joyner−Halenda (BJH) method. At 20 Pa, the films exhibit a surface area of 37 m^2/g and a porosity of around 68%. The derivative curve featuring the evolution of pore volume as a function of pore diameter shows a bimodal distribution with two types of pore size at 10 and 40 nm (see Supporting Information). By contrast, the 40 Pa films display solely one type of mesopores for which the diameter is intermediate at around 30 nm. The surface area increases to 86 m^2/g while the porosity attains 79%. For comparison, the widely used mesoporous film made of acidic nanocrystalline anatase TiO_2 shows similar characteristics with a BET surface area of 86 m^2/g, film porosity of 67% and pore size of 20 nm (without $TiCl_4$ post-treatment of the films).[26]

Hierarchical mesostructures grown at 20 Pa were characterized as DSSC photoanodes. Reference photoanodes were prepared following the standard preparation described in ref 24 without scattering layer. All samples were sensitized with the recently developed heteroleptic thiophene-based sensitizer Na-Ru(4,1′-bis(5-hexylthiophen-2-yl)-2,2′-bipyridine)(4-carboxylic-acid-4′-carboxylate-2,2′-bipyridine) (thiocyanate)$_2$, coded as C101.[4] Closely related to the amphiphilic Z907Na family, the C101 combines both the advantages of greater molar extinction coefficient (ε = 17 500 L·mol^{-1}·cm^{-1}) and red-shifted metal-to-ligand charge transfer (MLCT) response owing to the increased donor strength of the ancillary ligand which causes the destabilization of the metal t_{2g} orbitals ($\lambda_{(MLCT)}$ = 547 nm). To prevent bunching of the trees during solvent evaporation,[27] we carefully rinsed the sensitized electrodes with hexane so as to reduce interactions between neighboring branches.

First, we show in Figure 3a the (J−V) characteristics collected for a typical 2 μm photoanode under different incident light intensity exposure (100, 50, 10, and 0% equivalent sunlight illumination, A.M. 1.5 G condition). A power conversion efficiency (PCE) of 3.1% was achieved, despite the very low film thickness with J_{sc} = 5.3 mA/cm^2,

DOI: 10.1021/nl101198b | Nano Lett. 2010, 10, 2562--2567

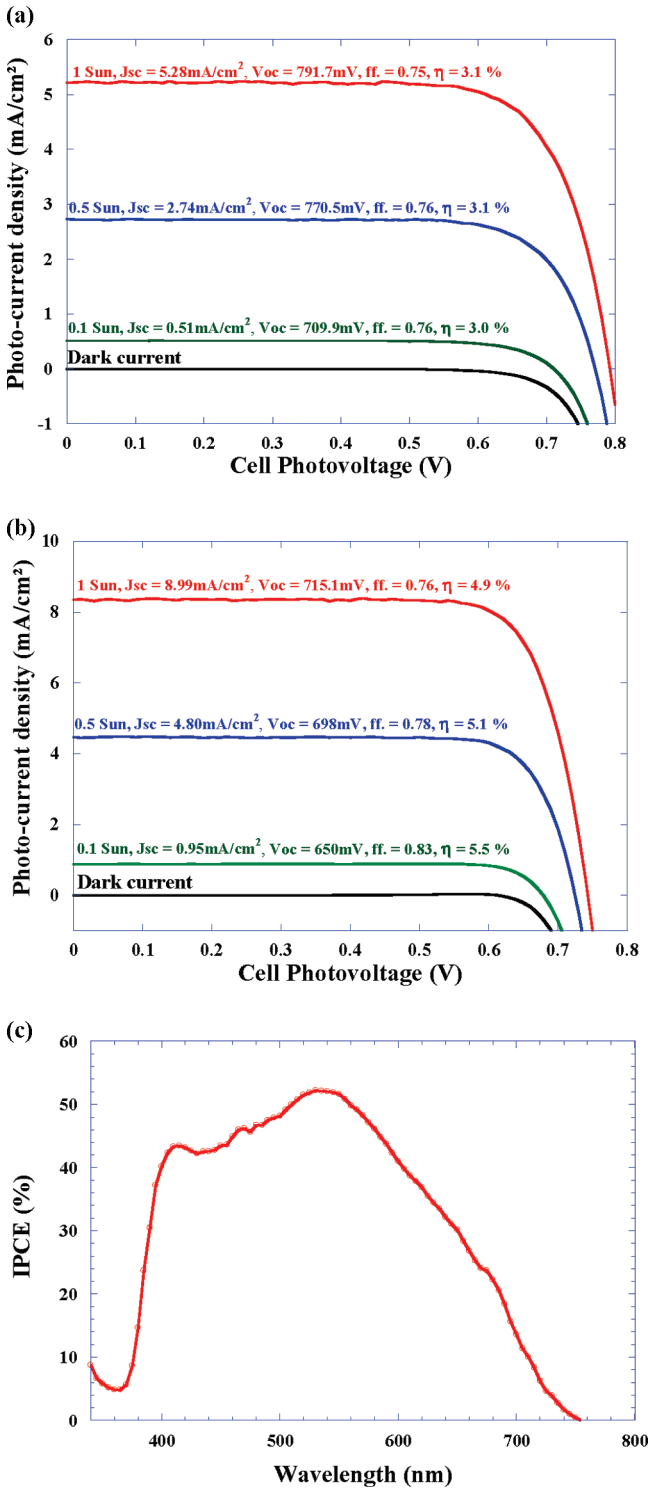

FIGURE 3. (*J*−*V*) characteristics recorded at different light illumination for PLD films prepared at background oxygen pressures of 20 Pa with different thicknesses (a) 2 μm, (b) 7 μm, and (c) IPCE spectrum of the (20 Pa, 7 μm) sample.

V_{oc} = 792 mV and fill factor (ff) = 0.75. By increasing film thickness to 7 μm, we were able to enhance the PCE to 4.9% at 1 sun and 5.5% at 0.1 sun owing to a noticeable improvement in the short circuit current density (J_{sc} = 9.0 mA/cm^2) while maintaining the fill factor as high as 76% (Figure 3b). The incident photon-to-electron conversion efficiency (IPCE) curve is reported in Figure 3c. The photons absorption and conversion to electrons is observed in the wavelength range between 400 and 750 nm with a maximum of IPCE of 53% at 536 nm. The result of IPCE integration is in good correlation with the 9 mA/cm^2 short circuit current density recorded when using our solar simulator. However, as a result of the increased thickness that induces more pathways for electron recombination, the cell photovoltage dropped to 715 mV, value which lies below those obtained on a typical 7 + 5 μm type configuration,[4] beads of TiO_2,[28] or optimized photoanode configuration with the opto-electronic properties of C101 for high-efficiency cells.[5] Increasing even further the thickness to 12−13 μm yields a decrease in performances, particularly due to an uncompensated loss of the V_{oc} in the case of the PLD-grown films. In Table 1, we summarize the obtained results and compare PV performance of the novel architecture with standard photoanode composed of acidic 20 nm based anatase TiO_2 particles. While ff and V_{oc} of the 20 Pa series are similar or even better than the reference, short circuit current is roughly half, yielding to overall lower power conversion efficiency. The inferior current could be related to the lower roughness factor of PLD grown photoanode with respect to the reference one. These photovoltaic performances obtained using PLD-grown films are comparable to the recent achievements reported by Grimes and co-workers on nanotube arrays deposited on TCO[16] (for comparable film thicknesses) and are superior to the anodization approach on Ti substrate where the cell has to be illuminated by the counter electrode side.[10−14] Nevertheless, the PCE of the PLD photoanodes still lags below the 7.4 and 8.4% obtained on standard 7 μm thick electrode composed of acidic 20 nm based TiO_2 particles before and after $TiCl_4$ post-treatment, respectively.[29]

TABLE 1. Photovoltaic Characteristics of C101 Dye onto PLD-Made Photoanode and Nanocrystalline Film of Different Thicknesses

	V_{oc} (mV)	J_{sc} (mA/cm)^2	FF	η (%)
PLD 2 μm	791.7	5.28	0.75	3.1
PLD 7 μm	715.1	8.99	0.766	4.9
PLD 13 μm	780	5.86	0.8	3.7
nc 2 μm	774	12.2	0.739	7
nc 7 μm	736	16.5	0.746	9.3
nc 13 μm	711	17	0.71	8.8

Interestingly, when studying the PLD-grown TiO_2 electrodes, we observe a significant overpotential increase for the tri-iodide reduction based on the voltamperograms recorded under dark condition using the Z960 electrolyte composition (1 M DMII, 50 mM LiI, 30 mM I_2, 0.5 M *tert*-butylpyridine and 0.1 M GuNCS in a solvent mixture of 85% acetonitrile with 15% valeronitrile by volume). This greater overpotential reaches 115 mV differences for the 20 Pa grown 2 μm thick films and about 20 mV for the 7 μm thick films.

DOI: 10.1021/nl101198b | *Nano Lett.* **2010,** *10,* 2562--2567

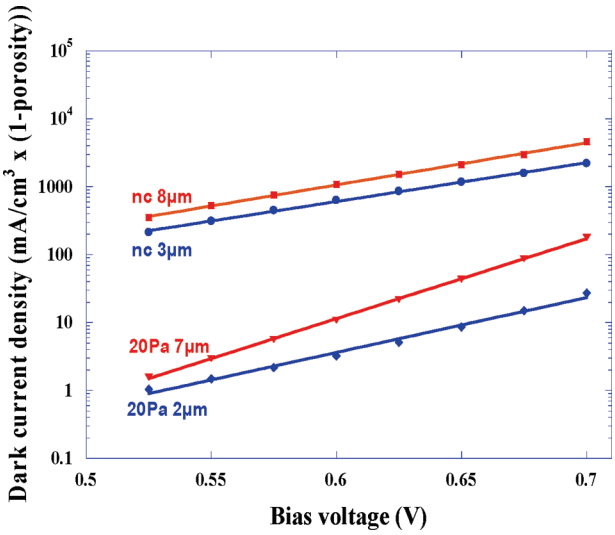

FIGURE 4. Comparison between standard nanocrystalline film and PLD-grown films on the evolution of dark current density normalized by the film thickness and porosity as a function of bias voltage.

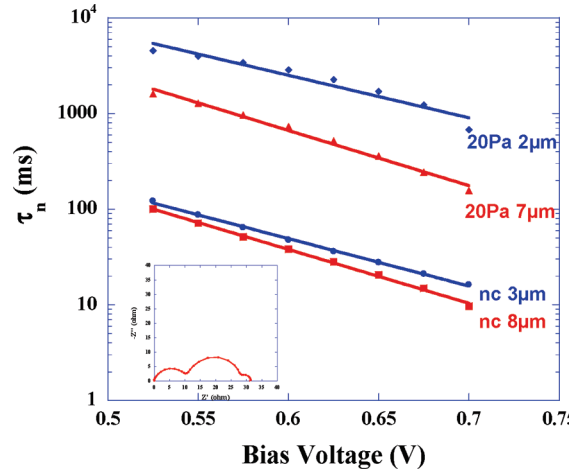

FIGURE 5. Evolution of the electron lifetime as a function of bias voltage for standard nanocrystalline film and PLD-grown films.

The evolution of the dark current density normalized for the different film thicknesses and porosities as a function of the bias voltage is reported in Figure 4. Regardless of the film used, the current generated by the reduction of tri-iodide follows an exponential dependence with bias voltage in agreement with the Butler−Volmer relationship. As a result of the higher overpotential, the generation of cathodic current at the surface of the PLD photoanode is attenuated by one to two orders of magnitude in comparison to the standard nanocrystalline film. In addition, although the current values reported were normalized by the film thickness, one can notice a discrepancy in the current generated suggesting a nonlinearity behavior for both types of film. In other words, the particles composing the top of the photoanode and those close to the TCO are not equivalent from an electrochemical point of view, and the top particles are more electrochemically active toward tri-iodide reduction. This implies that electron transport throughout TiO_2 nanoparticles is faster than tri-iodide mass transport in the mesopores. Note also in the Tafel-like plot the difference in slope between the 7 and the 2 μm PLD-made thick films which reflects the fact that the cathodic electronic transfer coefficient (α_{cath}) depends on the film thickness conversely to the standard nanocrystalline film ($\alpha_{cath} \approx 3.40 \times 10^{-5}$). This α_{cath} increased (from 3.75×10^{-5} to 4.23×10^{-5}) can be explained by the cross sectional SEM observations that suggest increased interface with the electrolyte when the film growths thicker (Figure 1).

To gain better insight in the dynamics of interfacial charge transfer processes, we have used the electrochemical impedance spectroscopy technique in dark condition using a two-electrode configuration. This powerful tool allows discriminating the different interfacial electrochemical processes as a function of their relaxation time constant. In liquid-junction DSSC, the Nyquist plot generally features three semicircles that reflect the charge transfer resistance at the counter electrode in the kHz region, the Nernst-type impedance due to electron transport across the nanocrystalline titania layer and their recapture by tri-iodide in the Hz region and finally the so-called finite-Warburg impedance relative to the tri-iodide mass transport in the mHz region[30,31] (example of EIS spectrum shown in Figure 5 inset). All spectra recorded were simulated using Zview software with an equivalent circuit that depicts a general transmission line electrical model established originally to describe the macroscopic homogeneous porous electrode model.[32] The electron lifetime value (τ_n) or "recombination time" was derived from the product between the resistance of recombination and the capacitance for the electron transfer. The semilogarithmic plot shown in Figure 5 presents the linear dependence of the electron lifetime as a function of the bias voltage for the different films. The hierarchical assembly exhibits a significantly higher electron lifetime, by more than 1 order of magnitude, in comparison to the reference mesoporous TiO_2 nanocrystalline film. This could account for a better charge collection efficiency when using this tree morphology as similarly experienced on films composed of perpendicular array of TiO_2 nanotubes.[10] It is noteworthy that the reduction of the electron lifetime when increasing the thickness which appears more pronounced in the case of the PLD films. This point can be related to an increased α_{cath} value as we discussed above. It also gives a plausible explanation on the unusual significant loss of V_{oc}, that is, from 792 to 715 mV, while the film thickness was only augmented to 7 μm. In addition to the positive aspect of delayed recombination dynamics when using this forest-like photoanode film, we have also attempted to quantify how such morphology could affect the tri-iodide diffusion coefficient in the mesopores when using a solvent-free, ternary eutectic melt, ionic liquid-based electrolyte (2.9 M of DMII/EMII (1:1), 2.1 M of EMITCB, 0.22 M I_2, 0.09 M GuNCS and 0.44 M of *N*-butyl benzimidazole).[33] At first, we have evaluated the intrinsic apparent tri-iodide diffusion coefficient by using electrochemical imped-

DOI: 10.1021/nl101198b | *Nano Lett.* **2010,** *10,* 2562--2567

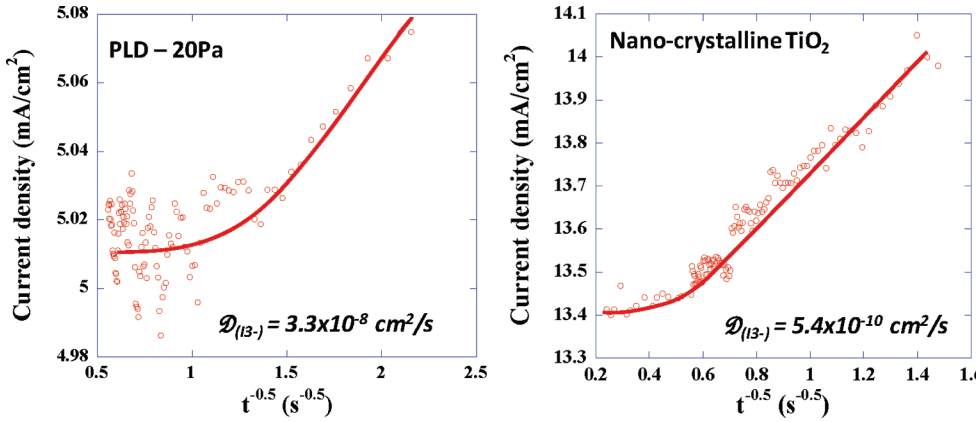

FIGURE 6. Evolution of current density as a function of $t^{-1/2}$ obtained from chrono-amperometric method under 100 mW/cm^2 illumination for standard nanocrystalline and PLD 7 μm thick films.

ance spectroscopy on TCO-Pt/electrolyte/Pt-TCO symmetric cells. As a result, we have deduced from the simulation of the Warburg impedance and more particularly from the slope of the plot $R = f(\omega^{-1/2})$ the apparent tri-iodide diffusion coefficient to be $D(I_3^-) = 4.10^{-8}$ cm^2/s. This is about 1 order of magnitude lower than the value reported using rotating disk ultramicroelectrode method.[34] To compare the apparent tri-iodide diffusion coefficient in the mesopores of PLD-grown and standard nanocrystalline 7 μm thick films, we have used the short-time approximation of the Cottrell's law using chrono-amperometry method on DSSC cells illuminated at 100 mW/cm^2. Owing to the kinetic control of the cell by mass transport, the chrono-amperogram shows an exponential decrease of the current with time before achieving a steady state. Figure 6 represents the evolution of the current density as a function of $t^{-1/2}$. The linear dependence verifies Cottrell's law from which the apparent diffusion coefficient of tri-iodide is extracted from the slope of the curve. Although Cottrell's law is verified for a short period on the PLD-film, it is extremely remarkable that the apparent tri-iodide diffusion coefficient herein evaluated of ca. $D(I_3^-) = 3.3 \times 10^{-8}$ cm^2/s is extremely close to the one determined by electrochemical impedance spectroscopy on TCO-Pt symmetric cell. This suggests that the hierarchical assembly of TiO_2 nanoparticles produced by PLD does not hinder the mass transport. This is in contrast with the case of the nanocrystalline film for which the mass transport seems more drastically affected by the mesopores in light of the 2 orders of magnitude fall in the apparent tri-iodide diffusion coefficient evaluated to $D(I_3^-) = 5.4 \times 10^{-10}$ cm^2/s.

To conclude, we have shown in this study that by a careful control of the PLD growth parameters, it is possible to mimic down to the nanoscale the morphology of trees that nature has designed for photosynthesis. In combination with the high molar extinction coefficient heteroleptic C101 dye, we were able to achieve 3.1% power conversion efficiency for only 2 μm thick films and 5% for films 7 μm thick. On the basis of electrochemical impedance spectroscopy, we have demonstrated that this architecture impairs the electron back reaction with tri-iodide. In particular, we have found that electron lifetime can be increased by more than 1 order of magnitude in comparison to the benchmark mesoporous TiO_2 films composed of acidic 20 nm based nanocrystalline particles. On the other hand, we have also demonstrated in this study that this hierarchical structure does not hinder mass transport of tri-iodide in solvent-free ionic liquid electrolyte. We are currently working on optimizing film porosity and surface area to increase the roughness factor, while maintaining similar morphology to further improve light harvesting ability of such films and as a consequence to push further the power conversion efficiency.

Acknowledgment. F.S., P.C., and M.G. acknowledge financial support of this work by FP7 EU project "ROBUST DSC" Grant agreement 212792. C.D. wishes to thank the Royal Society for funding. C.D., G.D., F.D.F., C.S.C., V.R., A.L.B., and C.E.B. are grateful for support from the IP3 project of the sixth Framework Program of the European Commission: ESTEEM (Enabling Science and Technology for European Electron Microscopy, Contract No. 0260019).

Supporting Information Available. Experimental section, pore volume as a function of pore diameter deduced from N_2 desorption experiment for films deposited at 20 and 40 Pa. This material is available free of charge via the Internet at http://pubs.acs.org.

REFERENCES AND NOTES

(1) Fujishima, A.; Honda, K. *Nature* **1972**, *238*, 37.
(2) O'Regan, B.; Graetzel, M. *Nature* **1991**, *353*, 737.
(3) Chiba, Y.; Islam, A.; Wanatabe, Y.; Komiya, R.; Koide, N.; Han, L. *Jpn. J. Appl. Phys.* **2006**, *45* (25), L638–L640.
(4) Gao, F.; Wang, Y.; Shi, D.; Zhang, J.; Wang, M.; Jing, X.; Humphry-Baker, R.; Wang, P.; Zakeeruddin, S. M.; Graetzel, M. *J. Am. Chem. Soc.* **2008**, *130*, 10720–10728.
(5) Sauvage, F.; Decoppet, J.-D.; Comte, P.; Nazeeruddin, Md. K.; Zakeeruddin, S. M.; Graetzel, M. submitted for publication.
(6) Kuang, D.; Klein, C.; Ito, S.; Moser, J.-E.; Humphry-Baker, R.; Evans, N.; Duriaux, F.; Graetzel, C.; Zakeeruddin, S. M.; Graetzel, M. *Adv. Mater.* **2007**, *19*, 1133–1137.
(7) Han, L.; Fukui, A.; Chiba, Y.; Islam, A.; Komiya, R.; Fuke, N.; Koide, N.; Yamanaka, R.; Shimizu, M. *Appl. Phys. Lett.* **2009**, *94*, No. 013305.

DOI: 10.1021/nl101198b | *Nano Lett.* **2010,** *10,* 2562–2567

(8) Frank, A. J.; Kopidakis, N.; Van de Lagemaat, J. *Coord. Chem. Rev.* **2004**, *248*, 1165–1179.
(9) Graetzel, M. *Inorg. Chem.* **2005**, *44* (20), 6841.
(10) Zhu, K.; Neale, N. R.; Miedaner, A.; Frank, A. J. *Nano Lett.* **2007**, *7*, 69–74.
(11) Prakasam, H. E.; Shankar, K.; Paulose, M.; Varghese, O. K.; Grimes, C. A. *J. Phys. Chem. C* **2007**, *111*, 7235–7241.
(12) Jennings, J. R.; Ghicov, A.; Peter, L. M.; Schmuki, P.; Walker, A. B. *J. Am. Chem. Soc.* **2008**, *130*, 13364–13372.
(13) Kim, D.; Ghicov, A.; Albu, S. P.; Schmuki, P. *J. Am. Chem. Soc.* **2008**, *130*, 16454–16455.
(14) Mor, G. K.; Kim, S.; Paulose, M.; Varghese, O. K.; Shankar, K.; Basham, J.; Grimes, C. A. *Nano Lett.*, in press.
(15) Feng, X.; Shankar, K.; Varghese, O. K.; Paulose, M.; Latempa, T. J.; Grimes, C. A. *Nano Lett.* **2008**, *8*, 3781–3786.
(16) Varghese, O. K.; Paulose, M.; Grimes, C. A. *Nat. Nanotechnol.* **2009**, *4*, 592.
(17) Zhang, Q. F.; Dandeneau, C. S.; Zhou, X. Y.; Cao, G. Z. *Adv. Mater.* **2009**, *21*, 4087–4108.
(18) Qian, J.; Liu, P.; Xiao, Y.; Jiang, Y.; Cao, Y.; Ai, X.; Yang, H. *Adv. Mater.* **2009**, *21*, 3663–3667.
(19) Chrisey, ; Hubler, *Pulsed Laser Deposition of Thin Films*; Wiley: New York, 1994.
(20) Infortuna, A.; Harvey, A. S.; Gauckler, L. J. *Adv. Funct. Mater.* **2008**, *18*, 127.
(21) Di Fonzo, F.; Tonini, D.; Li Bassi, A.; Bottani, C. E.; Gastaldi, D.; Vena, P.; Contro, R. *Appl. Phys. A* **2008**, *93*, 765–769.
(22) Dellasega, D.; Facibeni, A.; Di Fonzo, F.; Bogana, M.; Polissi, A.; Conti, C.; Ducati, C.; Casari, C. S.; Li Bassi, A.; Bottani, C. E. *Nanotechnology* **2008**, *19*, 475602.
(23) Bailini, A.; Di Fonzo, F.; Fusi, M.; Casari, C. S.; Li Bassi, A.; Russo, V.; Baserga, A.; Bottani, C. E. *Appl. Surf. Sci.* **2007**, *253*, 8130.
(24) Di Fonzo, F.; Bailini, A.; Russo, V.; Baserga, A.; Cattaneo, D.; Beghi, M. G.; Ossi, P. M.; Casari, C. S.; Li Bassi, A.; Bottani, C. E. *Catal. Today* **2006**, *116*, 69–73.
(25) Di Fonzo, F.; Casari, C. S.; Russo, V.; Brunella, M. F.; Li Bassi, A.; Bottani, C. E. *Nanotechnology* **2009**, *20*, No. 015604.
(26) Ito, S.; Murakami, T. N.; Comte, P.; Liska, P.; Graetzel, C.; Nazeeruddin, Md. K.; Graetzel, M. *Thin Solid Film* **2008**, *516* (14), 4613–4619.
(27) Zhu, K.; Vinzant, T. B.; Neale, N. R.; Frank, A. J. *Nano Lett.* **2007**, *7* (12), 3739–3746.
(28) Sauvage F., Chen D., Comte P., Huang F., Cheng Y. B., Caruso R. A., Graetzel M. *ACS Nano*, in press.
(29) Chandiram A. K., Sauvage F., Comte P., Casas-Cabanas M., Graetzel M. submitted for publication.
(30) Bisquert, J. *J. Phys. Chem. B* **2002**, *106*, 325.
(31) Kuang, D.; Klein, C.; Zhang, Z.; Ito, S.; Moser, J. E.; Zakeeruddin, S. M.; Graetzel, M. *Small* **2007**, *12*, 2094.
(32) Wang, Q.; Ito, S.; Graetzel, M.; Fabregat-Santiago, F.; Mora-Sero, I.; Bisquert, J.; Bessho, T.; Imai, H. *J. Phys. Chem. B* **2006**, *110*, 25210.
(33) Bai, Y.; Cao, Y.; Zhang, J.; Wang, M.; Li, R.; Wang, P.; Zakeeruddin, S. M.; Graetzel, M. *Nat. Mater.* **2008**, *7*, 626–630.
(34) Zakeeruddin, S. M.; Graetzel, M. *Adv. Funct. Mater.* **2009**, *19*, 2187–2202.
(35) Bando, K. K.; Mitsuzuka, Y.; Sugino, M.; Sugihara, H.; Sayama, K.; Arakawa, H. *Chem. Lett.* **1999**, 853.

DOI: 10.1021/nl101198b | *Nano Lett.* **2010,** *10,* 2562--2567